WSe_2 as a saturable absorber for multi-gigahertz *Q*-switched mode-locked waveguide lasers [Invited]

Ziqi Li (李子琦)[1], **Rang Li** (李 让)[1], **Chi Pang** (逄 驰)[1], **Yuxia Zhang** (张玉霞)[2], **Haohai Yu** (于浩海)[2], **and Feng Chen** (陈 峰)[1,*]

[1]*School of Physics, State Key Laboratory of Crystal Materials, Shandong University, Jinan 250100, China*
[2]*State Key Laboratory of Crystal Materials and Institute of Crystal Materials, Shandong University, Jinan 250100, China*
**Corresponding author: drfchen@sdu.edu.cn*

Received October 27, 2018; accepted December 7, 2018; posted online January 29, 2019

Graphene and other extraordinary two-dimensional materials together with recent advances in optical modulators have set the foundations for the widespread applications of next-generation optoelectronic devices. In this work, we report on the high-performance fundamentally mode-locked waveguide laser modulated by chemical-vapor-deposition-grown WSe_2 as a saturable absorber. By incorporating a WSe_2 sample into a monolithic Nd:YVO_4 waveguide platform, 6.526 GHz picosecond pulsed laser generation has been achieved at the wavelength of 1 μm with pulse duration of 47 ps.

OCIS codes: 160.4236, 140.4050, 140.3540, 230.7370.
doi: 10.3788/COL201917.020013.

Since the discovery of graphene, the emerging two-dimensional (2D) materials have been the subject of intense research, owing to their distinctive and intriguing optical properties[1–5]. Graphene possesses excellent nonlinear optical properties, e.g., ultrafast relaxation time and ultrabroadband absorption properties. Based on these, graphene has been recognized as one of the most effective optical modulators in ultrafast laser generation[6,7]. The intense research of graphene related saturable absorbers (SAs) has led to a rise of interest in exploring the saturable properties, as well as their application in pulsed laser generation based on many other extraordinary 2D materials[8–11]. As new functional materials for optoelectronic applications, transition metal dichalcogenides (TMDCs), denoted as MX_2 (M: Mo or W and X: S, Se, or Te), have recently been extensively studied with superb nonlinear optical properties, such as strong light–material interaction, broadband optical response, ultrafast recovery time, and controllable optoelectronic properties[12]. With these extraordinary nonlinear optical properties, TMDCs have been successfully demonstrated to be efficient optical modulators in the regime of *Q*-switched or mode-locked lasers within various laser systems, such as a fiber laser, waveguide laser, and bulk laser[13–19]. Among TMDCs, the most frequently used SAs are MoS_2 and WS_2. Tungsten diselenide (WSe_2) is one of the typical TMDCs that has been recently discovered with superb nonlinear saturable absorption properties[20,21]. However, the application of WSe_2 in laser generation is still at its early age, and there are limited reports on a 1 μm pulsed laser as well as waveguide lasers.

Optical waveguides are microstructures in dielectric materials that could confine light propagation within microscale volumes[22,23]. Based on laser crystals, waveguide lasers could be realized and have provided a solution to the problem that has plagued scientists on how to fabricate miniature and functional laser sources in integrated photonics chips. Compared with conventional laser sources, waveguide lasers have the advantages of small size, high stability, and easy integration of other optical devices, such as fibers. With the tight confinement of the light field, enhanced lasing performances could be realized in waveguide structures, such as reduced laser threshold value and higher slope efficiency. In addition, the intensity profiles of the emitted laser could be designed in a controllable way[24]. Based on the monolithic waveguide configuration, 2D materials have been widely applied as SAs in both *Q*-switched and mode-locked lasers operating in a wide spectral range within diverse laser systems[25–28].

Multi-gigahertz (GHz) mode-locked lasers have been the subject of intense research from academics for a large range of applications in a number of fields, including high-speed optical communication, frequency comb spectroscopy, biological imaging, and nonlinear microscopy[29–31]. Particularly, fundamentally mode-locked laser systems operating with the repetition rate value up to a GHz are favorable according to the applications in related fields. Based on the monolithic waveguide platform, research on the GHz mode-locked lasers is an emerging and fast-growing field. Based on a graphene SA and a thulium-doped yttrium aluminum garnet (Tm:YAG) waveguide, Ren *et al.* realized 2 μm *Q*-switched mode locking with output power of 6.5 mW and pulse rate of 7.8 GHz[32]. Mary *et al.* report on 1.5 GHz graphene *Q*-switched mode-locked waveguide lasing with slope efficiency of 48% at 1039 nm[33]. Recently, Thorburn *et al.* achieved a graphene-based waveguide laser with repetition rate of 5.9 GHz and up to 170 mW output power[34]. Most recently, the GHz picosecond waveguide laser

generation has been reported based on several other 2D materials (e.g., graphene, MoS_2, and Bi_2Se_3)[35]. In the case of continuous-wave mode locking (CWML), based on Ti: sapphire waveguides, Grivas *et al.* achieved graphene mode-locked ultrashort pulse lasing with 41.4 fs pulse width and 21.25 GHz repetition rate[36]. GHz CWML waveguide lasers have also been realized based on graphene and $ReSe_2$ by Okhrimchuk *et al.* and Li *et al.* respectively[37,38]. It is interesting to find the mode-locked performances based on a WSe_2 SA in the waveguide system at the wavelength of 1 μm.

In this Letter, we report on the realization of GHz Q-switched mode-locked lasing in a monolithic Nd:YVO_4 waveguide platform. Modulated by a WSe_2 SA, 6.526 GHz picosecond laser pulses have been demonstrated with pulse duration of 47 ps. This work indicates that WSe_2 could be applied as an efficient optical modulator in on-chip ultrafast photonics.

The monolithic waveguide platform is fabricated in a four-sided polished Nd:YVO_4 laser crystal (1 at. % Nd^{3+} ions), and its dimension is $10(x)$ mm × $10(y)$ mm × $2(z)$ mm. The miniature structures in the crystal were produced by femtosecond (fs) laser writing using a 120 fs Ti:sapphire regenerative amplifier (Spitfire, Spectra Physics). During the laser irradiation process, the sample is placed on a computer-controlled three-dimensional (3D) translation stage. Through program control, a number of low refractive index tracks with desired circular geometry are written, forming the low-loss cladding waveguide with the diameter of 50 μm. More details about Nd:YVO_4 cladding waveguides fabrication can be found in Ref. [39].

The WSe_2 sample is a commercial product (supplied by 6Carbon technology) and customized to be monolayer by the technique of chemical vapor deposition (CVD) on a 10 mm × 10 mm optical polished Al_2O_3 thin film substrate. The atomic force microscopy (AFM) measurement is carried out in the tapping mode by the Bruker Dimension Icon AFM system in air at room temperature. Figure 1a shows the AFM topological image, and Fig. 1b illustrates the height profiles, indicating the monolayer nature of the CVD-grown WSe_2 sample. The Raman spectrum is measured and shows pronounced peaks at 250.7 and 258.8 cm^{-1}, corresponding to the in-plane E^1_{2g} and out-of-plane A_{1g} modes of 2H-WSe_2, respectively. The optical photograph of the WSe_2 sample is shown in the inset of Fig. 1c. The linear absorption properties of the WSe_2 sample are investigated by a UV visible (Vis) near-infrared (NIR) spectrophotometer (UV-1800, Shimadzu). Figure 1d illustrates the linear absorption spectrum of the WSe_2 sample and Al_2O_3 thin film substrate as a function of laser wavelength from the Vis to NIR spectral range. Superb linear absorption can be found in the WSe_2 sample from the Vis towards the NIR band, showing its potential application in a broadband SA. The bonding configurations as well as chemical composition of the WSe_2 layer are further analyzed by high-resolution X-ray photoelectron spectroscopy (HR-XPS) using an

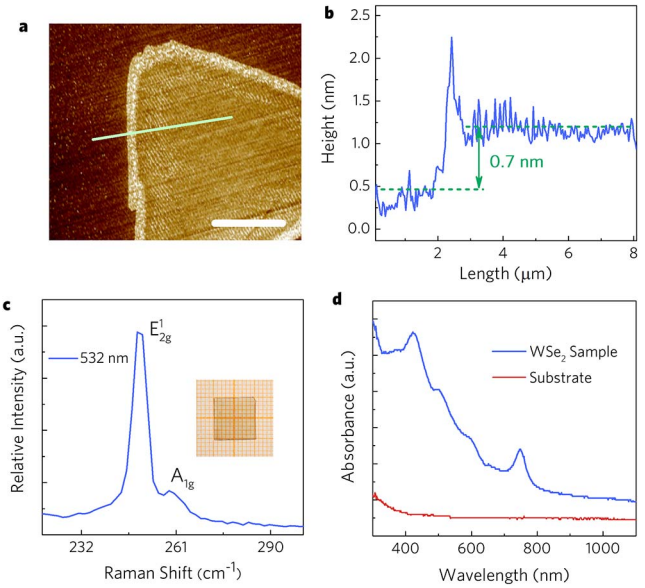

Fig. 1. a, The AFM image of the WSe_2 sample. b, The height profile image. c, The Raman spectrum under the excitation of 532 nm, and the inset is the optical image of the WSe_2 sample. d, The linear absorption spectra of WSe_2 and the substrate.

ESCALAB 250Xi XPS (Thermo Fisher Scientific, USA). In this measurement, monochromated Al Kα X-rays are employed to be the irradiation source, and the analyzer pass energy is 30 eV. As shown in Fig. 2a, the typical peaks located at 32.15 and 34.35 eV are attributed to W $4f^{7/2}$ and W $4f^{5/2}$ binding energies of W^{4+}. Figure 2b shows the bonding configurations of Se with peak locations at 54.45 and 55.3 eV, which could be assigned to $3d^{5/2}$ and $3d^{3/2}$, respectively. The HR-XPS spectrum is in good accordance with previous reports of CVD-grown highly crystalline WSe_2. With further analysis, we could quantitatively obtain the ratio (R) between Se and W atoms to be approximately 2:1, indicating the successful preparation and high quality of the CVD-grown WSe_2 sample.

WSe_2 has superb nonlinear optical properties (relatively small bandgap and broadband saturable absorption), and the related Z scan as well as pump–probe measurement has been reported in detail with modulation depth $\Delta T = 0.83\%$ and saturation intensity $I_{sat} \approx 14.1$ GW/cm^2 in our previous report[21]. The pulsed waveguide laser generation in this work was carried out by using the end-face coupling configuration, as illustrated in Fig. 3. The waveguide laser system was pumped by a 808 nm Ti:sapphire laser (Coherent MBR-110) with excellent beam quality of (TEM_{00}) and superior stability. In order to couple the pump laser into the cladding waveguide efficiently, an end-face coupling configuration was employed by using a spherical lens with 25 mm focal length. The input mirror M1 was anti-reflection (AR) coated at 808 nm (>99% transmission) and high-reflection (HR) coated at 1064 nm (>99.9% reflectivity). A 20 times objective lens with numerical aperture of 0.4 was then used to collect the emitted laser. In order to eliminate

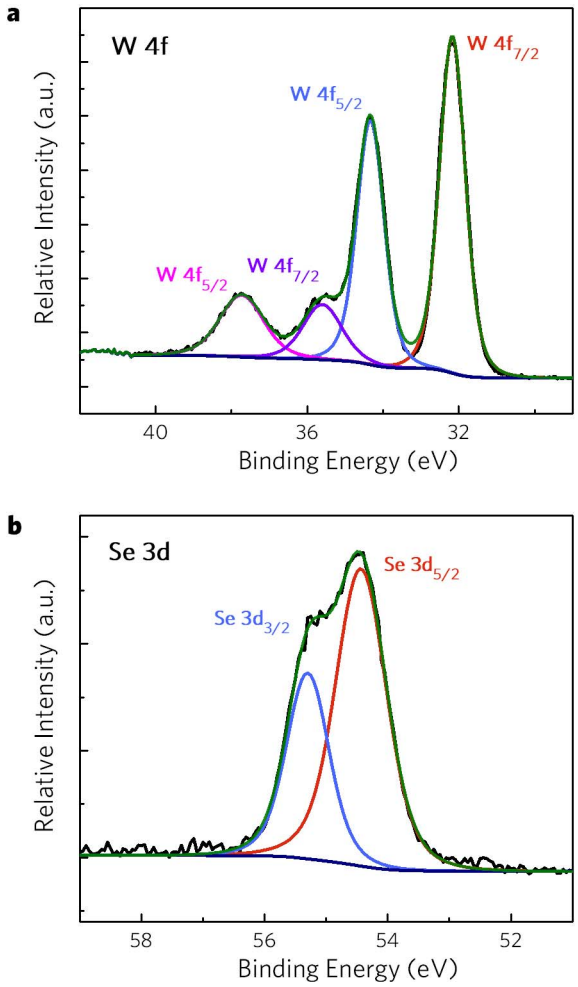

Fig. 2. High-resolution X-ray photoelectron spectroscopy (HR-XPS) of CVD-grown WSe_2 sample. a, The HR-XPS spectrum of W 4f. b, The HR-XPS spectrum of Se 3d.

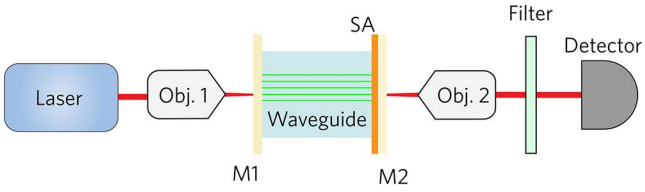

Fig. 3. Schematic diagram of the experimental setup of Q-switched mode-locked waveguide laser modulated by the WSe_2 SA.

the influence of unwanted pump light, the collected generated laser passed through an 850 nm cut-on wavelength long pass filter (Thorlabs, FEL0850). We further confirmed the absence of pump light from the spectrum analyzer. At the end of the experimental setup, a fiber launch system was used to efficiently couple the generation free-space laser into a single mode fiber. The fiber is connected to an ultrafast photodetector and real time digital oscilloscope with excellent performances.

With CVD-grown WSe_2 as an SA, Q-switched mode-locked pulsed lasing has been realized in a monolithic

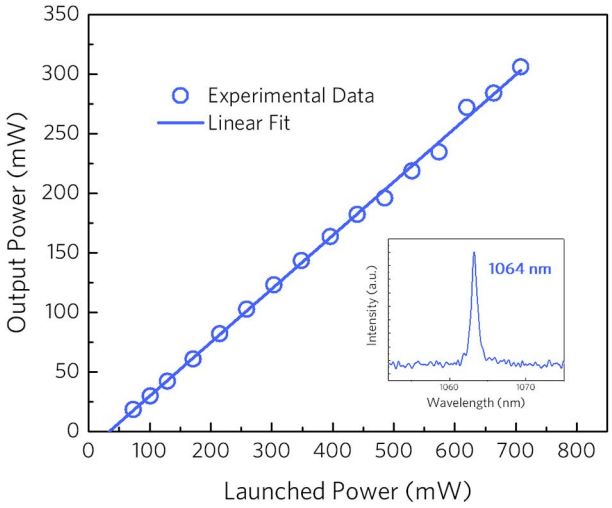

Fig. 4. Average output power as a function of the input power. The inset shows the emission spectrum of the waveguide laser modulated by WSe_2.

$Nd:YVO_4$ waveguide platform. Figure 4 shows the experimental data and its linear fitting of the output power versus pump power; a Q-switched mode-locked waveguide laser has been obtained once the pump power exceeds the laser oscillation threshold of 34 mW. It can be found that the laser generated with the WSe_2 SA is with low laser threshold and high slope efficiency. Efficient Q-switched mode-locked waveguide laser emission has been achieved when the pump power is higher than the laser oscillation threshold of 34 mW with slope efficiency of 45%, reaching the maximum output power value of 306 mW under the pump power of 707 mW at TE polarization. As shown in the inset of Fig. 4, the central wavelength of the laser emission spectrum is located at 1064 nm, attributed to the Nd^{3+} ions main laser oscillation line ($^4F_{3/2}$ to $^4I_{11/2}$).

The mode-locked laser performances are recorded by a high-speed (25 GHz) InGaAs photodetector (New Focus, 1414 model) with 14 ps rise time, as well as a 25 GHz electrical bandwidth digital oscilloscope (Tektronix, MSO 72504DX) with 16 ps rise time. Figure 5a demonstrates the single Q-switched envelope containing numbers of mode-locked picosecond pulses on the nanosecond (40 ns/div) time scale under the pump power of 420 mW. It can be seen the mode-locked laser is almost fully modulated. The Q-switched envelopes at a larger time scale (1 μs/div) are shown in Fig. 5b, illustrating uniform and consistent Q-switched mode-locked envelopes. Figure 5c depicts the measured mode-locked pulsed trains within the envelope on the picosecond timescale of 250 ps/div. As demonstrated in Fig. 6a, the pulse duration of a single mode-locked pulse is measured to be as short as 47 ps. The radio frequency (RF) spectrum has also been measured and is shown in Fig. 6b. It can be seen that the mode-locked waveguide laser with a WSe_2 modulator operates at a fundamental repetition rate up to multi-GHz with the value of 6.526 GHz. Only one sharp peak has been

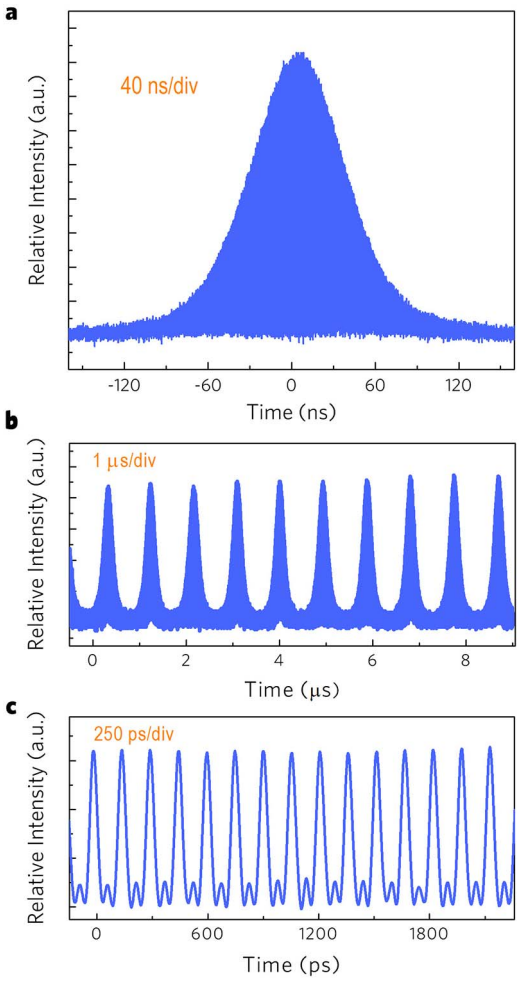

Fig. 5. a, The Q-switched envelope containing mode-locked pulses on 40 ns timescale. b, The Q-switched envelopes on a larger time scale of 1 μs. c, The recorded mode-locked pulse trains on the picosecond timescale.

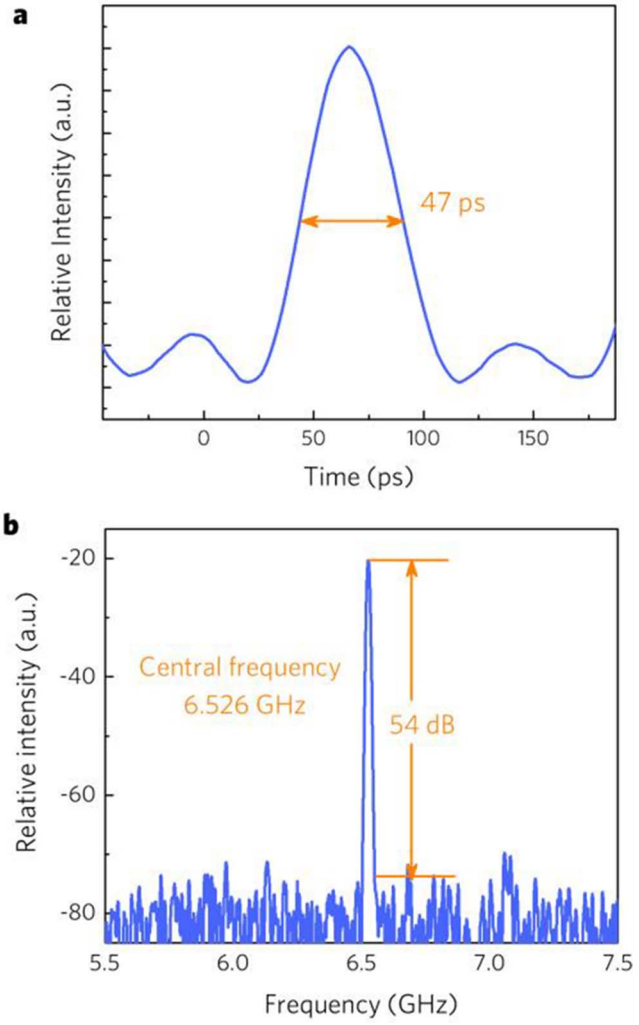

Fig. 6. a, Recorded single mode-locked pulse train. b, The measured RF spectrum.

Table 1. Comparison of GHz Q-Switched Mode-locked Waveguide Lasers Based on 2D Materials

	Parameters						
2D Materials	Fabrication Method	Gain Media	Wavelength (nm)	Pulse Width (ps)	Frequency (GHz)	SNR (dB)	Ref.
Graphene	LPE	Tm:YAG	1943.5	~70	7.8	–	[32]
Graphene	CVD	Ho:YAG	2091	~100	5.9	–	[34]
Graphene	LPE	Yb:BG	1039	1.06	1.5	~50	[33]
Graphene	CVD	Yb:Er-doped glass	1535	~70	6.8	~30	[40]
Graphene	CVD	Nd:YVO_4	1064	52	6.5	55	[35]
MoS_2	CVD	Nd:YVO_4	1064	43	6.5	51	[35]
Bi_2Se_3	CVD	Nd:YVO_4	1064	26	6.5	59	[35]
WSe_2	CVD	Nd:YVO_4	1064	47	6.526	54	This work

observed from the RF spectrum. In addition, the signal-to-noise ratio (SNR) is up to 54 dB, indicating the realized mode-locked waveguide lasing operation, is relatively stable. Only the *Q*-switched mode-locking operation has been observed with relative constant pulse duration and repetition rate. In addition, there is no observed damage to the WSe_2 during the measurement within our pump range. Table 1 summarizes recent advances of *Q*-switched mode-locked waveguide laser operating at the gigahertz repetition rate. The employment of WSe_2 saturable absorber has provided more choices beyond graphene to achieve miniature laser sources with high repetition rate.

The fundamental repetition rate of the mode-locked waveguide laser operation can be further confirmed with the following equation:

$$f_{\text{rep}} = \frac{c}{2nl}, \tag{1}$$

where c is the light speed, n is the waveguide refractive index, and l is the length of the cavity. Taking into account the approximately 11 mm laser cavity length, the fundamental repetition rate can be estimated to be as high as ~6.5 GHz, which is in good agreement of the fundamentally mode-locked lasing results in this work.

In conclusion, we have experimentally demonstrated multi-GHz *Q*-switched mode-locking operation in a monolithic Nd:YVO_4 waveguide platform modulated by monolayer WSe_2 as the SA. The mode-locked waveguide laser operates at a fundamental repetition frequency of 6.526 GHz, and the pulse width is measured to be as short as 47 ps. These results indicate promising applications of CVD-grown WSe_2 for future optoelectronic applications in integrated optics.

This work was supported by the National Natural Science Foundation of China (No. 61775120).

References

1. Z. Sun, A. Martinez, and F. Wang, Nat. Photon. **10**, 227 (2016).
2. A. Autere, H. Jussila, Y. Dai, Y. Wang, H. Lipsanen, and Z. Sun, Adv. Mater. **30**, 1705963 (2018).
3. Y. Ying, Y. Yang, W. Ying, and X. Peng, Nanotechnology **27**, 332001 (2016).
4. S. C. Dhanabalan, J. S. Ponraj, H. Zhang, and Q. Bao, Nanoscale **12**, 6410 (2013).
5. B. Wang, H. Yu, H. Zhang, C. Zhao, S. Wen, and J. Wang, IEEE Photon. J. **6**, 1501007 (2014).
6. Q. Bao, H. Zhang, Y. Wang, Z. Ni, Y. Yan, Z. X. Shen, K. P. Loh, and D. Y. Tang, Adv. Funct. Mater. **19**, 3077 (2009).
7. Q. Bao and K. P. Loh, ACS Nano **6**, 3677 (2012).
8. X. Jiang, S. Liu, W. Liang, S. Luo, Z. He, Y. Ge, H. Wang, R. Cao, F. Zhang, Q. Wen, J. Li, Q. Bao, D. Fan, and H. Zhang, Laser Photon. Rev. **12**, 1700229 (2018).
9. Y. Ge, Z. Zhu, Y. Xu, Y. Chen, S. Chen, Z. Liang, Y. Song, Y. Zou, H. Zeng, S. Xu, H. Zhang, and D. Fan, Adv. Opt. Mater. **6**, 1701166 (2018).
10. Z. Luo, D. Wu, B. Xu, H. Xu, Z. Cai, J. Peng, J. Weng, S. Xu, C. Zhu, F. Wang, Z. Sun, and H. Zhang, Nanoscale **8**, 1066 (2016).
11. B. Guo, Chin. Opt. Lett. **16**, 020004 (2018).
12. K. F. Mak and J. Shan, Nat. Photon. **10**, 216 (2016).
13. J. Wang, Z. Jiang, H. Chen, J. Li, J. Yin, J. Wang, T. He, P. Yan, and S. Ruan, Photon. Res. **6**, 535 (2018).
14. J. Wang, Z. Jiang, H. Chen, J. Li, J. Yin, J. Wang, T. He, P. Yan, and S. Ruan, Opt. Lett. **42**, 5010 (2017).
15. M. Lin, Q. Peng, W. Hou, X. Fan, and J. Liu, Opt. Laser Technol. **109**, 90 (2019).
16. Y. Xue, Z. Xie, Z. Ye, X. Hu, J. Xu, and H. Zhang, Chin. Opt. Lett. **16**, 020018 (2018).
17. H. Zhang, S. B. Lu, J. Zheng, J. Du, S. C. Wen, D. Y. Tang, and K. P. Loh, Opt. Express **22**, 7249 (2014).
18. B. Chen, X. Zhang, K. Wu, H. Wang, J. Wang, and J. Chen, Opt. Express **23**, 26723 (2015).
19. C. Cheng, H. Liu, Y. Tan, J. R. Vázquez de Aldana, and F. Chen, Opt. Express **24**, 10385 (2016).
20. W. Liu, M. Liu, J. Yin, H. Chen, W. Lu, S. Fang, H. Teng, M. Lei, P. Yan, and Z. Wei, Nanoscale **10**, 7971 (2018).
21. Y. Tan, X. Liu, Z. He, Y. Liu, M. Zhao, H. Zhang, and F. Chen, ACS Photon. **4**, 1531 (2017).
22. F. Chen and J. R. Vázquez de Aldana, Laser Photon. Rev. **8**, 251 (2014).
23. F. Chen, Laser Photon. Rev. **6**, 622 (2012).
24. T. Calmano, A. G. Paschke, S. Muller, C. Krankel, and G. Huber, Opt. Express **21**, 25501 (2013).
25. C. Wieschendorf, J. Firth, L. Silvestri, S. Gross, F. Ladouceur, M. J. Withford, D. J. Spence, and A. Fuerbach, Opt. Express **25**, 1692 (2017).
26. G. Palmer, S. Gross, A. Fuerbach, D. G. Lancaster, and M. J. Withford, Opt. Express **21**, 17413 (2013).
27. X. Jiang, S. Gross, M. J. Withford, H. Zhang, D. I. Yeom, F. Rotermund, and A. Fuerbach, Opt. Mater. Express **8**, 3055 (2018).
28. Z. Li, N. Dong, C. Cheng, L. Xu, M. Chen, J. Wang, and F. Chen, Opt. Mater. Express **8**, 3055 (2018).
29. S. Hakobyan, V. J. Wittwer, P. Brochard, K. Gurel, S. Schilt, A. S. Mayer, U. Keller, and T. Sudmeyer, Opt. Express **25**, 20437 (2017).
30. S. W. Chu, T. M. Liu, and C. K. Sun, Opt. Express **11**, 933 (2003).
31. H. M. Oubei, J. R. Duran, B. Janjua, H. Y. Wang, C. T. Tsai, Y. C. Chi, T. K. Ng, H. C. Kuo, J. H. He, M.-S. Alouini, G. R. Lin, and B. S. Ooi, Opt. Express **23**, 23302 (2015).
32. Y. Ren, G. Brown, R. Mary, G. Demetriou, D. Popa, F. Torrisi, A. C. Ferrari, F. Chen, and A. K. Kar, IEEE J. Sel. Top. Quantum Electron. **21**, 395 (2015).
33. R. Mary, G. Brown, S. J. Beecher, F. Torrisi, S. Milana, D. Popa, T. Hasan, Z. Sun, E. Lidorikis, S. Ohara, A. C. Ferrari, and A. K. Kar, Opt. Express **21**, 7943 (2013).
34. F. Thorburn, A. Lancaster, S. McDaniel, G. Cook, and A. K. Kar, Opt. Express **25**, 26166 (2017).
35. Z. Li, Y. Zhang, C. Cheng, H. Yu, and F. Chen, Opt. Express **26**, 11321 (2018).
36. C. Grivas, R. Ismaeel, C. Corbari, C. Huang, D. W. Hewak, P. Lagoudakis, and G. Brambilla, Laser Photon. Rev. **12**, 1800167 (2018).
37. A. G. Okhrimchuk and P. A. Obraztsov, Sci. Rep. **5**, 11172 (2015).
38. Z. Li, N. Dong, Y. Zhang, J. Wang, H. Yu, and F. Chen, APL Photon. **3**, 080802 (2018).
39. Z. Li, C. Cheng, N. Dong, C. Romero, Q. Lu, J. Wang, J. R. Vázquez de Aldana, Y. Tan, and F. Chen, Photon. Res. **5**, 406 (2017).
40. A. Choudhary, S. Dhingra, B. D'Urso, P. Kannan, and D. P. Shepherd, IEEE Photon. Technol. Lett. **27**, 646 (2015).